Unbalance Response of a Magnetic Suspended Dual-rotor System

Wang Dongxiong[a,b] Wang Nianxian[a,b] Chen Kuisheng[a,b] Ye Chun[a,b] Ran Shaolin[c] Wu Huachun[c] Song Chunsheng[c]

[a]The Key Laboratory for Metallurgical Equipment and Control of Ministry of Education, Wuhan University of Science and Technology, NO. 947, Heping Avenue, Qingshan District, CT, Wuhan 430081, China

[b]Hubei Key Laboratory of Mechanical Transmission and Manufacturing Engineering, Wuhan University of Science and Technology, NO. 947, Heping Avenue, Qingshan District, CT, Wuhan 430081, China

[c]School of Mechanical and Electronic Engineering, Wuhan University of Technology

***Abstract*: The magnetic suspended dual-rotor system (MSDS) applied in more electric aero-engine can eliminate the wear and lubrication system of mechanical bearings and solve the vibration control issue of system effectively, which provides the possibility to improve the performance of aero-engine significantly. This research focuses on the unbalance response of the MSDS. First, a structure of dual-rotor system supported by two active magnetic bearings (AMBs) and two permanent magnetic bearings (PMBs) is proposed. With classic PD control adopted, the bearing characteristics of AMBs are modeled as the equivalent stiffness and equivalent damping, and the PMBs are modeled as elastic support with stiffness. Then, the Riccati transfer matrix method with good numerical stability is used to establish the unbalance response model of the MSDS. Next, the interaction between inner and outer rotors is analyzed with single rotor imbalance excitation, and the unbalance response of the MSDS is investigated with dual-rotor imbalance excitation. In addition, a simple and effective approach to avoid simultaneous excitations by both inner and outer rotors is pointed out. Finally, experiments on the unbalance response of a magnetic suspended single-rotor system is conducted to validate some theoretical analysis of the MSDS.**

***Keywords*: Magnetic suspended dual-rotor system, Unbalance response, Riccati transfer matrix method**

Ⅰ. INTRODUCTION

Due to many advantages of magnetic bearings (MBs) over conventional bearings such as contactless operation, low power consumption, lubrication-free operation, controllable bearing dynamic properties and extended life, the substitution of MBs for mechanical bearings to support dual-rotor systems can greatly reduce the system complexity and the engine weight, save the cost, optimize the engine structure, and obtain higher reliability and maintainability [1]. Therefore, MSDS provides the possibility to improve engine performance significantly.

However, with inevitable existence of rotor imbalance induced by material inhomogeneity, machining and installation error, periodic unbalance vibration occurs. Although the rotor imbalance can be reduced by off-line balancing, residual imbalance still exists due to the working conditions changed and the limited correction accuracy. Besides, the unbalance vibration forces transfers to the pedestal and produces unwanted vibration, which will affect the system performance. Therefore, research on synchronous vibration force suppression has attracted wide attention.

Gao et al. [2] analyzed the beat vibration phenomenon of an AMB system by solving the dynamic equations, adjusted the control current to change the generalized dynamic stiffness of AMBs in order to weaken the beat vibration, and finally verified it by experiments. Fu et al. [3] identified imbalances by genetic algorithms to balance the rotor based on the transient response of rotor accelerated starting in an AMB system. Chen et al. [4] presented a design for a fuzzy gain tuning mechanism dealing with the problem of unbalance vibration problem in an AMB system based upon a self-tuning fuzzy PID-type controller, and showed that the proposed scheme allowed for a remarkable improvement in reducing vibration and an efficient reduction of the shaft displacement in an unbalanced AMB system by experiments. A double-loop compensation design approach based on the AMB was proposed by Chen et al. [5] to achieve automatic balancing within the entire

operating speed range, simulation and experiment results well demonstrated effectiveness of the approach, which was unaffected by the attenuation of power amplifier at high speeds. Furthermore, to suppress the unbalance vibration without angular velocity information, Chen et al. [6] presented a novel modified adaptive notch filter with phase shift in the AMB system, and achieved the effectiveness and the adaptive characteristics of the proposed method on the elimination of synchronous controlled current in a widely operating speed range by simulation and experiments on an AMB driveline system. Zheng et al. [7] explored a novel auto-balancing method for the magnetic suspended rotor in the motor driveline system based on the synchronous rotating frame transformation, and demonstrated a significant effect on the synchronous vibration suppression of the rotor suspended by AMBs. Even though many control strategies have been proposed and successfully applied to suppress synchronous unbalance vibration of the rotor, their application target is mainly for the magnetic suspended single rotor systems.

Due to high efficiency and stall margin, dual-rotor systems have been widely used in air turbine starters, propfans and aero-engines [8]. There are relatively a few of researches on the unbalance response of a dual-rotor system at present. An extended transfer matrix procedure in complex variables was developed by K. Gupta et al. [9] for obtaining unbalance response of dual-rotor systems, and experimental results were in reasonable agreement with theoretical results. Based on the transfer matrix method and corresponding boundary conditions, the steady state unbalance responses of the counter-rotating dual-rotor system were analyzed by Hu et al. [10], and the changing characteristics of the disks' orbits and the centroids' locations were studied experimentally. Chen et al. [11] investigated the vibration analysis of the whole aero-engine, and studied the sensitivity of unbalance response as well as the transient vibration laws caused by sudden addition of imbalance. It can be seen that researches on the unbalance response of dual-rotor systems are mainly focused on the modeling and the basic dynamic characteristics of the unbalance response of dual-rotor systems supported by mechanical bearings. Moreover, there are few literatures that report the unbalance response of a MSDS. Nevertheless, research on the unbalance response of a MSDS is important for reducing the vibration and noise and improving the reliability and stability of the system.

In this research, unbalance response of MSDS with two PMBs and two AMBs is investigated. Based on the system dynamic model established by Riccati transfer matrix method, the interaction between inner and outer rotors is analyzed with single rotor imbalance excitation, and the unbalance response of the MSDS is studied with dual-rotor imbalance excitation. A simple and effective measure to avoid simultaneous excitations by both inner and outer rotors is proposed. Finally, the experimental results of unbalance response of a magnetic suspended single-rotor system verify some theoretical analysis.

Ⅱ. MSDS MODEL

The structure schematic and theoretical model of the MSDS are presented in Fig. 1, where two coaxial rotors interlinked through two PMBs acting as inter-shaft bearings, and the outer rotor is levitated by two AMBs. In this dual-rotor system, one end of the outer rotor is connected to the motor through an elastic diaphragm coupling. Since the elastic diaphragm coupling allows a certain axial deviation and deflection angle, the axial DOF of the outer rotor can be regulated. Therefore, the outer rotor can be regarded as a 4-DOF rotor, and the same for the inner rotor. The total lengths of inner and outer rotors are 0.34m and 0.285m, respectively. The main parameters of disks attached to the dual-rotor system are listed in Table 1.

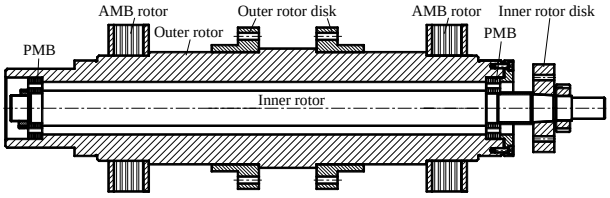

(a) MSDS structure

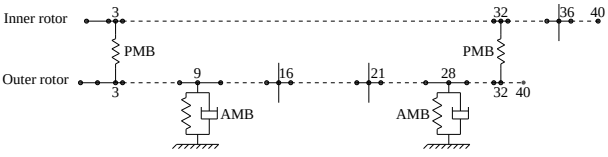

(b) MSDS theoretical model

Figure 1 Structure and theoretical model of the MSDS

Table 1 Main parameters of disks

No.	Station	Mass (kg)	Polar Moment of Inertia (kg·m^2)	Transverse Moment of Inertia (kg·m^2)
1	36	0.167	5.73×10^{-5}	2.86×10^{-5}
2	16	0.323	5.07×10^{-4}	2.54×10^{-4}

3	21	0.323	5.07×10^{-4}	2.54×10^{-4}

E=2.09×10[11] Pa, μ=0.269, ρ=7850kg/m^3

A. AMB MODELING

For either AMBs or traditional mechanical bearings, bearing characteristics are the foundation for the rotor dynamics analysis. In mechanical bearings, the commonly used parametric representations for bearing characteristics are the stiffness and the damping, which are also used for AMBs, namely, the equivalent stiffness and the equivalent damping. Compared with mechanical bearing system, the AMB system is open loop unstable and feedback control is needed for rotor levitation. Whatever control strategy is adopted in the AMB system, its bearing characteristics can always be represented by the equivalent stiffness and equivalent damping. When the proportional derivative (PD) control strategy is adopted, the form becomes more explicit. Moreover, the PD algorithm is easy to use, and has strong applicability and mature technology. Therefore, it has been widely used in the AMB system, usually as the main controller of the system [12, 13]. PD control is adopted in this research for simplification.

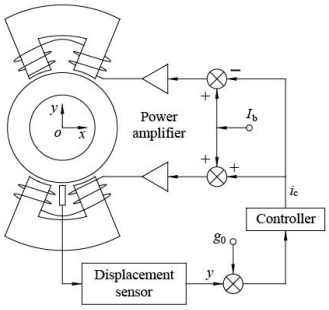

(a) Basic control loop

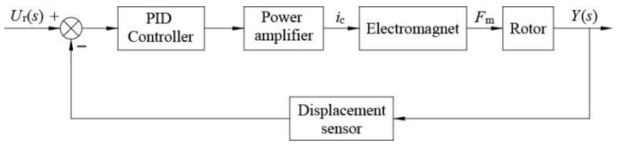

(b) Control block diagram

Figure 2 Basic control loop and control block diagram of the AMB

For a typical eight-pole radial AMB with differential drive mode, the basic magnetic bearing control loop and control block diagram in the y axis are shown in Fig. 2. According to Ref. [14-17], the equivalent stiffness k_e and equivalent damping d_e of the AMB can be expressed as

$$\begin{cases} k_e = k_i A_a A_s K_P - k_s \\ d_e = k_i A_a A_s K_D \end{cases} \quad (1)$$

where, K_P and K_D are the proportional and derivative coefficients. A_a and A_s are the gain of the power amplifier and the displacement sensor. k_s and k_i are the displacement stiffness and current stiffness coefficients of the AMB, and they are respectively given as

$$\begin{cases} k_s = \dfrac{\mu_0 A_p N^2 I_b^2 \cos\alpha}{g_0^3} \\ k_i = \dfrac{\mu_0 A_p N^2 I_b \cos\alpha}{g_0^2} \end{cases} \quad (2)$$

where, μ_0 is the permeability of vacuum. α is the angle between the central lines of the pole and pole-pair. A_p is the sectional area of one stator pole. N is the coil turn. I_b is the bias current of coils. g_0 is the nominal air-gap length of the AMB. In the following simulation, $\alpha=\pi/8$, $A_p=2.47\times10^{-4}$ m^2, N=160, I_b=3A, $g_0=5\times10^{-4}$ m, A_a=0.6 A/V, $A_s=8\times10^3$ V/m.

Considering the weak coupling effects of the AMB in x and y axes, the equivalent cross stiffness and equivalent cross damping are neglected. In this way, a rotor is supported by two AMBs. Each AMB support can be equivalent to two mutually perpendicular spring-damping structures. The spring-damping structure of each direction is completely independent. Therefore, the decentralized PD control is adopted in this research.

B. DYNAMIC MODEL OF MSDS

The mathematical model of the MSDS shown in Fig. 1(b) is represented by lumped masses a called stations which are connected by massless beam elements b. Bearings represented by bearing element c with four linearized coefficients are modeled as forces acting on the element a at the appropriate axial locations. For logical alignment and overall transfer of state variables, the inner rotor and outer rotor are both divided into 40 elements.

For simplicity, the following assumptions are made.

1) PMBs are modeled as elastic support with stiffness [18].

2) It is considered that the place where the magnetic force is applied is same as the place where the displacement is tested by the sensor.

3) The dynamic properties of AMBs are represented by four linearized coefficients, two (k_{ex}, k_{ey}) of which represent the stiffness properties and the other two (d_{ex}, d_{ey}) the damping properties.

4) Flexibilities and cross-coupling force effects of the foundation are ignored.

There are sixteen state variables, two deflections, two slopes, two bending moments, and two shear force components for inner and outer rotor, respectively. The

Riccati transfer matrix method divides the sixteen state variables $\boldsymbol{Z}$ into two groups, namely, $\boldsymbol{Z}=\{\boldsymbol{f}\ \boldsymbol{e}\}$, where $\boldsymbol{f}=\{M_{yi}\ Q_{xi}\ M_{xi}\ Q_{yi}\ M_{yo}\ Q_{xo}\ M_{xo}\ Q_{yo}\}^{\mathrm{T}}$, $\boldsymbol{e}=\{x_{\mathrm{i}}\ \theta_{yi}\ y_{\mathrm{i}}\ \theta_{xi}\ x_{\mathrm{o}}\ \theta_{yo}\ y_{\mathrm{o}}\ \theta_{xo}\}^{\mathrm{T}}$. The parameters are described in Nomenclature.

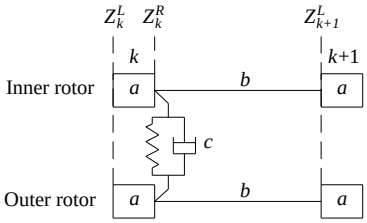

Figure 3 The kth elements of MSDS

Considering a dual-rotor system represented by N sectional matrices, the relationship of state vectors for the kth ($1\le k\le N$) element a shown in Fig. 3 is written by

$$\begin{Bmatrix} f \\ e \end{Bmatrix}_{kd}^{R} = \begin{bmatrix} D_{11} & D_{12} \\ D_{21} & D_{22} \end{bmatrix}_k \begin{Bmatrix} f \\ e \end{Bmatrix}_{kd}^{L} + \begin{Bmatrix} u_1 \\ u_2 \end{Bmatrix}_k \tag{3}$$

where, $\{\boldsymbol{f}\ \boldsymbol{e}\}_{kd}^{TR}$ and $\{\boldsymbol{f}\ \boldsymbol{e}\}_{kd}^{TL}$ are the right-hand and left-hand side state vectors of the kth element a, respectively. $\boldsymbol{u}_1=\{0\ U_{\mathrm{i}}\Omega_{\mathrm{i}}^2\ 0\ -U_{\mathrm{i}}\Omega_{\mathrm{i}}^2\ 0\ U_{\mathrm{o}}\Omega_{\mathrm{o}}^2\ 0\ -U_{\mathrm{o}}\Omega_{\mathrm{o}}^2\}^{\mathrm{T}}$, $\boldsymbol{u}_2=[0]_{8\times1}$. The superscript 'T' in $\{\boldsymbol{f}\ \boldsymbol{e}\}_{kd}^{TR}$ represents the state vectors transposed. The state vectors for the kth inner and outer rotor elements b are given as

$$\begin{Bmatrix} f \\ e \end{Bmatrix}_{kb}^{R} = \begin{bmatrix} B_{11} & B_{12} \\ B_{21} & B_{22} \end{bmatrix}_k \begin{Bmatrix} f \\ e \end{Bmatrix}_{kb}^{L} \tag{4}$$

where, $\{\boldsymbol{f}\ \boldsymbol{e}\}_{kb}^{TR}$ and $\{\boldsymbol{f}\ \boldsymbol{e}\}_{kb}^{TL}$ are the right-hand and left-hand side state vectors of the kth element b, respectively. When there is a coupling element, namely, the bearing element c, between inner and outer rotor elements a, the relationship of state vectors for the coupling element is expressed as

$$\begin{Bmatrix} f \\ e \end{Bmatrix}_{kc}^{R'} = \begin{bmatrix} R_{11} & R_{12} \\ R_{21} & R_{22} \end{bmatrix}_k \begin{Bmatrix} f \\ e \end{Bmatrix}_{kc}^{L'} \tag{5}$$

Considering that $\{\boldsymbol{f}\ \boldsymbol{e}\}_{kb}^{TR}=\{\boldsymbol{f}\ \boldsymbol{e}\}_{(k+1)d}^{TR}$, $\{\boldsymbol{f}\ \boldsymbol{e}\}_{kb}^{TL}=\{\boldsymbol{f}\ \boldsymbol{e}\}_{kc}^{TR'}$ and $\{\boldsymbol{f}\ \boldsymbol{e}\}_{kc}^{TL'}=\{\boldsymbol{f}\ \boldsymbol{e}\}_{kd}^{TR}$, omitting the subscript a, b and c, the relationship of state vectors for the kth elements a, b and c of the dual-rotor system is expressed as

$$\begin{Bmatrix} f \\ e \end{Bmatrix}_{k+1}^{L} = \begin{bmatrix} u_{11} & u_{12} \\ u_{21} & u_{22} \end{bmatrix}_k \begin{Bmatrix} f \\ e \end{Bmatrix}_{k}^{L} + \begin{Bmatrix} H_f \\ H_e \end{Bmatrix}_k \tag{6}$$

where,

$$\begin{bmatrix} u_{11} & u_{12} \\ u_{21} & u_{22} \end{bmatrix}_k = \begin{bmatrix} B_{11} & B_{12} \\ B_{21} & B_{22} \end{bmatrix}_k \begin{bmatrix} R_{11} & R_{12} \\ R_{21} & R_{22} \end{bmatrix}_k \begin{bmatrix} D_{11} & D_{12} \\ D_{21} & D_{22} \end{bmatrix}_k \tag{7}$$

$$\begin{Bmatrix} H_f \\ H_e \end{Bmatrix}_k = \begin{bmatrix} B_{11} & B_{12} \\ B_{21} & B_{22} \end{bmatrix}_k \begin{bmatrix} R_{11} & R_{12} \\ R_{21} & R_{22} \end{bmatrix}_k \begin{Bmatrix} u_1 \\ u_2 \end{Bmatrix}_k \tag{8}$$

The partitioned matrices $\boldsymbol{B}_{11}$, $\boldsymbol{B}_{12}$, $\boldsymbol{B}_{21}$, $\boldsymbol{B}_{22}$, $\boldsymbol{R}_{11}$, $\boldsymbol{R}_{12}$, $\boldsymbol{R}_{21}$, $\boldsymbol{R}_{22}$, $\boldsymbol{D}_{11}$, $\boldsymbol{D}_{12}$, $\boldsymbol{D}_{21}$ and $\boldsymbol{D}_{22}$ are described in the Appendix. It should be noted that if these constituents of partitioned matrices involving the support characteristics of inter-shaft bearings are all set equal to zero, the above equations will reduce to that of two uncoupled straight rotors. Omitting the superscript L, the expansion of Eq. (6) gives

$$\begin{cases} f_{k+1} = u_{11k} f_k + u_{12k} e_k + H_{fk} \\ e_{k+1} = u_{21k} f_k + u_{22k} e_k + H_{ek} \end{cases} \tag{9}$$

Introducing a Riccati transformation at station k,

$$f_k = S_k e_k + P_k \tag{10}$$

where, the Riccati transfer matrix $\boldsymbol{S}$ is a 8×8 matrix, $\boldsymbol{P}$ is a 8×1 vector. According to Eqs. (9) and (10), the recurrence formulas of $\boldsymbol{S}$, $\boldsymbol{P}$ and $\boldsymbol{e}$ are

$$S_{k+1} = \left(u_{11}S + u_{12}\right)_k \left(u_{21}S + u_{22}\right)_k^{-1} \tag{11}$$

$$P_{k+1} = \left(u_{11}P + H_f\right)_k - S_{k+1}\left(u_{21}P + H_e\right)_k \tag{12}$$

$$e_k = \left(u_{21}S + u_{22}\right)_k^{-1} e_{k+1} - \left(u_{21}S + u_{22}\right)_k^{-1}\left(u_{21}P + H_e\right)_k \tag{13}$$

Since the left-hand side boundary conditions are $f_1=0$ and $e_1\neq0$, the initial condition is $\boldsymbol{S}_1=0$ and $\boldsymbol{P}_1=0$. In the case of knowing $\boldsymbol{u}_{11}$, $\boldsymbol{u}_{12}$, $\boldsymbol{u}_{21}$, $\boldsymbol{u}_{22}$, $\boldsymbol{H}_e$ and $\boldsymbol{H}_f$ for each element, $\boldsymbol{S}_{k+1}$ and $\boldsymbol{P}_{k+1}$ can be obtained sequentially by using Eq. (11)-(12) repeatedly. For the right-hand side of station N, the relationship of the state vectors $\boldsymbol{f}_{N+1}$ and $\boldsymbol{e}_{N+1}$ is

$$f_{N+1} = S_{N+1}e_{N+1} + P_{N+1} \tag{14}$$

With the right-hand side boundary conditions $\boldsymbol{f}_{N+1}=0$ and $\boldsymbol{e}_{N+1}\neq0$, $\boldsymbol{e}_{N+1}$ is expressed as

$$e_{N+1} = -S_{N+1}P_{N+1} \tag{15}$$

By using Eq. (13), the state vector $\boldsymbol{e}_k$ ($1\le k\le N$) for each section can be calculated successively from right-hand side to left-hand side. Finally, the unbalance response of MSDS is obtained.

III. Unbalance response analysis

A. Unbalance responses of MSDS with single rotor excitation

Simulation on the MSDS shown in Fig. 1 is carried out to calculate the unbalance response with PMB stiffness 7×10^5 N/m, $K_{\mathrm{P}}=7$ and $K_{\mathrm{D}}=0.0003$. Ignoring the outer rotor imbalance and holding the outer rotor at speed 800 rad/s while varying the inner rotor speed, the responses of three disks excited by inner rotor imbalance 1×10^{-5} Kg·m are shown in Fig. 4(a). Similarly, the responses excited by only outer rotor imbalance 1×10^{-5} Kg·m are shown in Fig. 4(b) with inner rotor fixed at speed 800 rad/s while the outer rotor speed changed. In Fig. 4(a), three disks simultaneously achieve the maximum amplitudes at

specific speeds, which actually are the first three order critical speeds of MSDS excited by inner rotor. It indicates that when the inner rotor has a peak response at the critical speeds due to its own imbalance, the maximum response amplitudes of outer rotor occur at these speeds through the interaction of inter-shaft bearings. By comparing Fig. 4(a) and 4(b), the influence of the inner rotor imbalance on the outer rotor vibration amplitude is even greater than that of the outer rotor imbalance on the outer rotor itself. Relatively, the peak amplitude of the inner rotor caused by outer rotor imbalance is smaller than that of the inner rotor excited by the imbalance of inner rotor itself. In fact, this phenomenon is also observed at many other fixed inner and outer rotor speeds corresponding to Fig. 4(a) and 4(b).

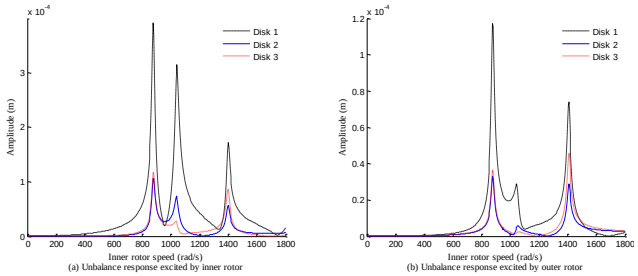

Figure 4 Unbalance response of MSDS with single rotor excitation

For MSDS, it is an important prerequisite to ensure the safe and reliable operation of aero-engine by reasonably configuring the critical speeds of rotor-bearing system. In the stage of engine overall scheme design, the rationality of the overall structure scheme is analyzed by estimating the critical speeds [11]. In a dual-rotor system, co-rotation and counter-rotation are two possible operation modes. The former one is with both rotors co-rotating, and the latter one is with the rotors counter-rotating with respect to each other. The typical case of co-rotation is considered in this research. The speed ratio r is defined as the ratio of outer rotor speed ω_0 to inner rotor speed ω_1, i.e., $r=\omega_0/\omega_1$.

Based on the above unbalance response analysis, the critical speed map of MSDS is depicted in Fig. 5(a). It should be noted that the solid lines and the dotted lines are excited by inner and outer rotors, respectively. The double hyphen line r=1.2 is the common working line, the critical speeds marked "*" are excited by inner rotor imbalance and the critical speeds marked "°" are excited by outer rotor imbalance. In the case of speed ratio r=1.2, the critical speeds of MSDS are given in Table 2.

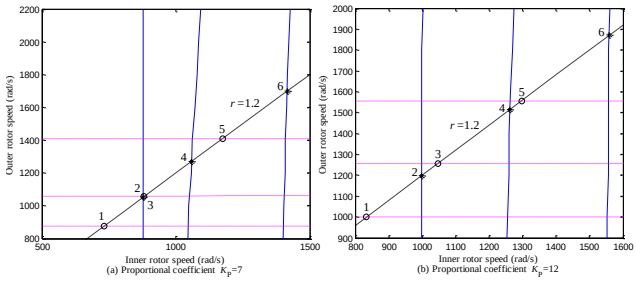

Figure 5 Critical speed maps of MSDS

Table 2 Critical speeds of MSDS with K_P=7

Number of points	Inner rotor speeds, rad/s	Outer rotor speeds, rad/s	Excitation by	Order of critical speeds
1	731.3	877.5	Outer rotor	1
2	877.5	1053.0	Inner rotor	1
3	881.3	1057.5	Outer rotor	2
4	1059.1	1270.9	Inner rotor	2
5	1173.8	1408.6	Outer rotor	3
6	1415.3	1698.3	Inner rotor	3

It is evident from Fig. 5(a) and Table 2 that in the case of r=1.2, the inner rotor excited first order critical speed pair (ω_1, ω_0)=(877.5, 1053.0) are approximately equal to the outer rotor excited second order critical speed pair (ω_1, ω_0)=(881.3, 1057.5), which indicates that the inner rotor excited critical speed and the outer rotor excited critical speed will occur simultaneously near the critical speed pairs. Near these critical speed pairs close to each other, the peak vibrations at the critical speeds of some specific orders are excited by both the inner and outer rotor imbalances. Thus, the dynamic behaviors of MSDS will become more complicated, which makes the design of control system more difficult. Therefore, the common working line must never pass through the intersections of the inner and outer rotor excitation lines. Further, long distances among the critical speed pairs are beneficial for the vibration performance of MSDS.

A simple and effective approach to avoid the simultaneous excitation is to choose appropriate the PD controller parameters. In the previous case, with K_P=12, the critical speed map of MSDS is shown in Fig. 5(b). Obviously, no common intersection of the three types of lines shows up. It should be noticed that this method can significantly change the critical speeds of MSDS.

B. Unbalance Responses of MSDS with Dual-Rotor Excitation

In general, both the inner and outer rotors are inevitably unbalanced in practical engineering application.

Thus, it is necessary to analyze the unbalance response of MSDS with imbalances in both inner and outer rotors. In the following simulation, we assume that the imbalances of disk 1 on the inner rotor and the disk 3 on the outer rotor are both 1×10^{-5} Kg·m. In this research, the MSDS is considered as a linear system, where the projections of unbalance forces acted on inner and outer rotor in horizontal or vertical plane are harmonic forces. From the perspective of vibration, the response of the whole MSDS is a superposition of the response vectors excited by two excitation forces. Therefore, firstly, the steady-state unbalance response can be calculated by the assumption that the imbalance only exists in inner rotor. Then, it is calculated by assuming that only the outer rotor is unbalanced. Finally, the steady-state unbalance response of the dual-rotor system with both inner and outer rotors unbalanced can be obtained by linear superposition of the unbalance response for the above two cases [10].

With PMB stiffness 7×10^5 N/m, K_P=7, K_D=0.0003 and r=1.2, the critical speeds of MSDS and the unbalance response of outer rotor disk 2 are shown in Table 2 and Fig. 6. Obviously, within the outer rotor speed 1800 rad/s, response peaks of the outer rotor occurs at the first three order critical speeds excited by outer rotor and the outer rotor speeds corresponding to the inner rotor excited critical speeds. As stated above, the outer rotor speed 1053.0 rad/s corresponding to the inner rotor excited first order critical speed is close to the outer rotor excited second order critical speed 1057.5 rad/s. Therefore, there are five peaks for the inner rotor unbalance response. It is the same for the inner rotor unbalance response, and its peaks occur at the inner speeds which are 1/r of outer rotor speeds.

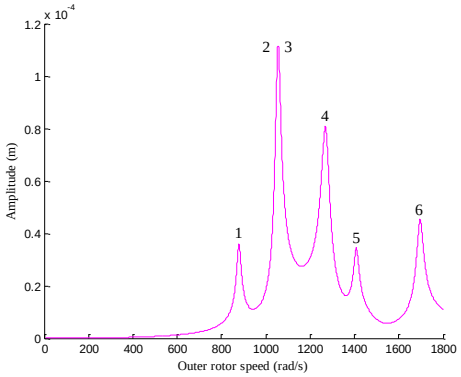

Figure 6 Unbalance response of MSDS with K_P=7

In the above case, with K_P=12, the critical speeds and the unbalance response of outer rotor disk 2 are shown in Table 3 and Fig. 7, respectively. The peaks are one-to-one correspondence to the critical speeds listed in Table 3 in despite of the 3rd and 5th peaks almost respectively covered by 2nd and 4th peaks. It is obvious that no peaks are overlapped. In this way, the MSDS will be excited by only one rotor imbalance at most when it runs at any pair of speeds, which will simplify the design of the AMB controller.

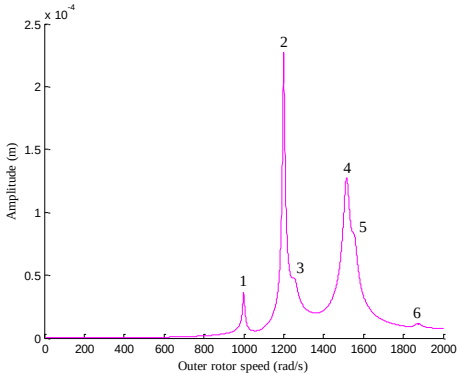

Figure 7 Unbalance response of MSDS with K_P=12

Table 3 Critical speeds of MSDS with K_P=12

Number of points	Inner rotor speeds, rad/s	Outer rotor speeds, rad/s	Excitation by	Order of critical speeds
1	833.23	999.88	Outer rotor	1
2	1000.3	1200.4	Inner rotor	1
3	1047.4	1256.9	Outer rotor	2
4	1263	1515.6	Inner rotor	2
5	1296.6	1555.9	Outer rotor	3
6	1560.1	1872.1	Inner rotor	3

Ⅳ. EXPERIMENT

In MSDS, it is possible that simultaneous excitations by inner and outer rotor unbalances can be avoided by reasonable selection of control parameters. In order to verify this, it is necessary to illustrate that the critical speeds of the system can be changed by reasonably selecting control parameters. Therefore, an experimental study on the unbalance response of a magnetic suspended single-rotor system is conducted. The magnetic suspended single-rotor system is shown in Fig.8, and the main parameters of the AMB system are given in Table 4.

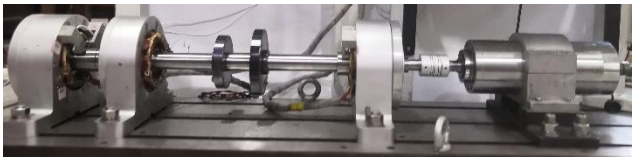

Figure 8 Test rig of a magnetic suspended single-rotor system

Table 4 Main parameters of AMB system

Parameters	Value
Maximum bearing capacity (N)	500
Nominal air-gap length (mm)	0.5
Radial gap between auxiliary bearing and rotor (mm)	0.25
Number of coil turns	192

Bias current	2.5
Sectional area of stator pole (mm^2)	697
Gain of the power amplifier (A/V)	1
Gain of the displacement sensor (V/mm)	5

In the case of K_P=2 and K_D=30, the theoretical calculations and experimental results of the unbalanced response are shown in Fig. 9(a). With the change of K_P=3, the results are shown in Fig. 9(b). Additionally, as stated above, a dual-rotor system gets degenerated into two straight rotors by setting all stiffness and damping coefficients of inter-shaft bearings equal to zero. The theoretical calculations of unbalance response for the magnetic suspended single-rotor system are given in Fig. 9.

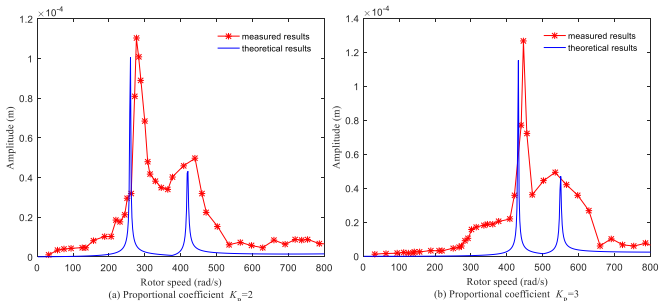

Figure 9 Unbalance responses of magnetic suspended single-rotor system

In Fig. 9(a) with K_P=2, two peaks occur at the speeds 277 rad/s and 440rad/s, which are the first two critical speeds. In Fig. 9(b) with K_P=3, two peaks occur at the speeds 446 rad/s and 534rad/s. Obviously, the critical speeds of the system can be changed by control parameter K_P. Furthermore, there is reasonable agreement between the theoretically predicted curves and the experimentally measured responses, which confirms the validity of some theoretical analysis of the MSDS. The error between the theoretical values and experimental values is mainly caused by the difference between the theoretical model and the experimental model.

V. CONCLUSIONS

In this research, unbalance response of a MSDS is investigated with the Riccati transfer matrix method, and the following conclusions are drawn.

The influence of the inner rotor imbalance excitation on the outer rotor is greater than that of the outer rotor imbalance excitation on the outer rotor itself, and the influence of the outer rotor imbalance excitation on the inner rotor is smaller than that of the inner rotor imbalance excitation on the inner rotor itself. It indicates that minimizing imbalance of the inner rotor is more important than that of the outer rotor from the view of system vibration performance. Furthermore, simultaneous excitation by both inner and outer rotor imbalances will complicate the dynamic behaviors of MSDS and makes the design of control system more difficult. It is pointed out that a simple and effective measure to avoid simultaneous excitation is to choose appropriate control parameters. Finally, experimental results of the unbalance response of a magnetic suspended single-rotor system confirm some theoretical analysis of the MSDS.

ACKNOWLEDGMENT

This work was supported by the National Natural Science Foundation of China (grant no. 51405351) and major projects of Natural Science Foundation of Hubei Province (grant no. 2014CFA013).

REFERENCES

[1] Zh. K. Wu, J. Li, R. J. Shi, "Current research status and key technology of more-electric aeroengine", *Advances in Aeronautical Science and Engineering*, vol. 3, no. 4, pp. 463-467, 2012.
[2] H. Gao, L. X. Xu, "Analysis of beat vibration for active magnetic bearing system", *Journal of Mechanical Engineering*, vol. 47, no. 13, pp. 104-112, 2012.
[3] Ch. Fu, "Non-weight tests dynamic balancing of flexible rotor based on accelerated unbalance response",*Journal of Northwestern Polytechnical University*, vol. 35, no. 5, pp. 898-904, 2017.
[4] K. Y. Chen, P. Ch. Tung, M. T. Tsai, et al., "A self-tuning fuzzy PID-type controller design for unbalance compensation in an active magnetic bearing", *Expert Systems with Applications*, vol. 36, no. 4, pp. 8560-8570, 2009.
[5] Chen, Q., G. Liu, S. Zheng, "Suppression of imbalance vibration for AMBs controlled driveline system using double-loop structure", *Journal of Sound and Vibration*, no. 337, pp. 1-13, 2015.
[6] Chen, Q., G. Liu, B, Han, "Unbalance vibration suppression for AMBs system using adaptive notch filter", *Mechanical Systems and Signal Processing*, no. 93, pp. 136-150, 2017.
[7] Zheng, S., et al., "Vibration Suppression control for AMB-supported motor driveline system using synchronous rotating frame transformation", *IEEE Transactions on Industrial Electronics*, vol. 62, no. 9, pp. 5700-5708, 2015.
[8] Ferraris, G., V. "Maisonneuve, M. Lalanne, "Prediction of the dynamic behavior of non-symmetrical coaxial co- or counter-rotating rotors", *Journal of Sound and Vibration*, vol. 195, no. 4, pp. 649-666, 1996.
[9] Gupta, K., K.D. Gupta, K. Athre, "Unbalance response of a dual rotor system theory and experiment", *Journal of Vibration and Acoustics*, vol. 115, no. 1, pp. 427-435, 1993.
[10] X. Hu, G. H. Luo, D. P. Gao, "Numerical analysis and experiment of counter- rotating dual- rotor' s steady- state response", *Journal of Aerospace Power*, vol. 22, no. 7, pp. 1044-1049, 2007.
[11] G. Chen, "Modeling and analysis of dual-rotor vibration for aero-engine", *Journal of Vibration Engineering*, vol. 24, no. 6, pp. 619-632, 2011.
[12] Anantachaisilp, P. Z. Lin, "An experimental study on PID tuning methods for active magnetic bearing systems", *International Journal of Advanced Mechatronic Systems*, vol. 5, no.2, pp. 146-154, 2013.
[13] Anantachaisilp, P. Z. Lin, "Fractional order PID control of rotor suspension by active magnetic bearings", *Actuators*, vol. 6, no.1, pp. 1-31, 2017.
[14] X. P. Wang, W. Wang, X. J. Wang, et al., "Research on dynamic characteristics of active magnetic bearing-rotor system", *Journal of Mechanical Engineering*, vol. 37, no. 11, pp. 7-12, 2001.
[15] Tang, J., B. Xiang, Y. Zhang, "Dynamic characteristics of the rotor in a magnetically suspended control moment gyroscope with active magnetic bearing and passive magnetic bearing". *Isa Transactions*, vol. 53, no. 4, pp. 1357-1365, 2014.

[16] K. J. Jiang, C. Sh. Zhu., Liangliang Chen, et al., "Multi-DOF rotor model based measurement of stiffness and damping for active magnetic bearing using multi-frequency excitation". *Mechanical Systems and Signal Processing*, vol. 60, no. 61, pp. 358-374, 2015.
[17] Zh. B. Wang, Ch. Mao, Ch. Sh. Zhu, "A design method of PID controllers for active magnetic bearings-rigid rotor systems", *Proceedings of the CSEE*, vol. 29, no. 00, pp. 1-9, 2017.
[18] N. X. Wang, D. X. Wang, K. Sh. Chen, et al., "Research on analytical model and design formulas of permanent magnetic bearings based on Halbach array with arbitrary segmented magnetized angle", *Journal of Magnetism and Magnetic Materials*, vol. 410, no.1, pp. 257-264, 2016.

APPENDIX

In section II, the partitioned matrices used to formulate the overall frequency equation are described herein. Due to the limitation of the space, the mathematical details have been omitted. The related parameters of formulae are described in Nomenclature.

$$D_{11} = D_{22} = R_{11} = R_{22} = I_{8\times 8} \tag{A.1}$$

where, $I_{8\times 8}$ represents the 8×8 identity matrix.

$$D_{21} = B_{12} = R_{21} = [0]_{8\times 8} \tag{A.2}$$

$$D_{12} = \begin{bmatrix} 0 & -J_{di}\omega^2 & 0 & -iJ_{pi}\Omega_i\omega & 0 & 0 & 0 & 0 \\ m_i\omega^2 - r_1 & 0 & 0 & 0 & 0 & 0 & 0 & 0 \\ 0 & iJ_{pi}\Omega_i\omega & 0 & -J_{di}\omega^2 & 0 & 0 & 0 & 0 \\ 0 & 0 & m_i\omega^2 - r_2 & 0 & 0 & 0 & 0 & 0 \\ 0 & 0 & 0 & 0 & 0 & -J_{do}\omega^2 & 0 & -iJ_{po}\Omega_o\omega \\ 0 & 0 & 0 & 0 & m_o\omega^2 - g_1 & 0 & 0 & 0 \\ 0 & 0 & 0 & 0 & 0 & iJ_{po}\Omega_o\omega & 0 & -J_{do}\omega^2 \\ 0 & 0 & 0 & 0 & 0 & 0 & m_o\omega^2 - g_2 & 0 \end{bmatrix} \tag{A.3}$$

where, $r_1=k_{ix}+ic_{ix}\omega$, $r_2=k_{iy}+ic_{iy}\omega$, $g_1= k_{ox}+ic_{ox}\omega$, $g_2= k_{oy}+ic_{oy}\omega$.

$$B_{21} = \begin{bmatrix} \gamma_{i2} & \gamma_{i3} & 0 & 0 & 0 & 0 & 0 & 0 \\ \gamma_{i1} & \gamma_{i2} & 0 & 0 & 0 & 0 & 0 & 0 \\ 0 & 0 & \gamma_{i2} & \gamma_{i3} & 0 & 0 & 0 & 0 \\ 0 & 0 & \gamma_{i1} & \gamma_{i2} & 0 & 0 & 0 & 0 \\ 0 & 0 & 0 & 0 & \gamma_{o2} & \gamma_{o3} & 0 & 0 \\ 0 & 0 & 0 & 0 & \gamma_{o1} & \gamma_{o2} & 0 & 0 \\ 0 & 0 & 0 & 0 & 0 & 0 & \gamma_{o2} & \gamma_{o3} \\ 0 & 0 & 0 & 0 & 0 & 0 & \gamma_{o1} & \gamma_{o2} \end{bmatrix} \tag{A.4}$$

where, $\gamma_{i1}=l_i/(EI_i)$, $\gamma_{i2}=l_i^2/(2EI_i)$, $\gamma_{i3}=l_i^3/(6EI_i)-l_i/(\alpha_iG_iA_i)$, $\gamma_{o1}=l_o/(EI_o)$, $\gamma_{o2}=l_o^2/(2EI_o)$, $\gamma_{o3}=l_o^3/(6EI_o)-l_o/(\alpha_oG_oA_o)$.

$$B_{11} = B_{22} = \begin{bmatrix} 1 & l_i & 0 & 0 & 0 & 0 & 0 & 0 \\ 0 & 1 & 0 & 0 & 0 & 0 & 0 & 0 \\ 0 & 0 & 1 & l_i & 0 & 0 & 0 & 0 \\ 0 & 0 & 0 & 1 & 0 & 0 & 0 & 0 \\ 0 & 0 & 0 & 0 & 1 & l_o & 0 & 0 \\ 0 & 0 & 0 & 0 & 0 & 1 & 0 & 0 \\ 0 & 0 & 0 & 0 & 0 & 0 & 1 & l_o \\ 0 & 0 & 0 & 0 & 0 & 0 & 0 & 1 \end{bmatrix} \tag{A.5}$$

$$R_{12} = \begin{bmatrix} 0 & 0 & 0 & 0 & 0 & 0 & 0 & 0 \\ -q_x & 0 & 0 & 0 & q_x & 0 & 0 & 0 \\ 0 & 0 & 0 & 0 & 0 & 0 & 0 & 0 \\ 0 & 0 & -q_y & 0 & 0 & 0 & q_y & 0 \\ 0 & 0 & 0 & 0 & 0 & 0 & 0 & 0 \\ q_x & 0 & 0 & 0 & -q_x & 0 & 0 & 0 \\ 0 & 0 & 0 & 0 & 0 & 0 & 0 & 0 \\ 0 & 0 & q_y & 0 & 0 & 0 & -q_y & 0 \end{bmatrix} \tag{A.6}$$

where, $q_x=k_{cx}+ic_{cx}\omega$, $q_y=k_{cy}+ic_{cy}\omega$.

NOMENCLATURE

A = cross-sectional area of shaft, m^2.
$\boldsymbol{B}_{11}$, $\boldsymbol{B}_{12}$, $\boldsymbol{B}_{21}$, $\boldsymbol{B}_{22}$ = 8×8 partitioned matrices.
c_{ix}, c_{iy} = damping coefficients of bearings to support inner rotor, N·s/m.
c_{ox}, c_{oy} = damping coefficients of bearings to support outer rotor, N·s/m.
c_{cx}, c_{cy} = inter-bearing damping coefficients, N·s/m.
$\boldsymbol{e}$ = 8×1 displacement vector with constituents: x_i, θ_{yi}, y_i, θ_{xi}, x_o, θ_{yo}, y_o, θ_{xo}.
$\boldsymbol{D}_{11}$, $\boldsymbol{D}_{12}$, $\boldsymbol{D}_{21}$, $\boldsymbol{D}_{22}$ = 8×8 partitioned matrices.
E = Young's modulus, Pa.
$\boldsymbol{f}$ = 8×1 force vector with constituents: M_{yi}, Q_{xi}, M_{xi}, Q_{yi}, M_{yo}, Q_{xo}, M_{xo}, Q_{yo}.
G = shear modulus, Pa.
i = imaginary unit.
J_p, J_d = polar and transverse moment of inertia, respectively, kg·m^2.
k_{ix}, k_{iy} = bearing stiffness coefficients for outer rotor, N/m.
k_{ox}, k_{oy} = bearing stiffness coefficients for outer rotor, N/m.
k_{cx}, k_{cy} = inter-bearing stiffness coefficients, N/m.
l_i, l_o = the inner and outer rotor length, respectively, m.
m_i, m_o = the inner and outer rotor mass, respectively, kg.
M_{yi}, M_{xi}, M_{yo}, M_{xo}= bending moments, N·m, 1st index is moment direction.
Q_{yi}, Q_{xi}, Q_{yo}, Q_{xo}= shear force, N, 1st index is shearing force direction.
$\boldsymbol{R}_{11}$, $\boldsymbol{R}_{12}$, $\boldsymbol{R}_{21}$, $\boldsymbol{R}_{22}$ = 8×8 partitioned matrices.
$\boldsymbol{u}_{11}$, $\boldsymbol{u}_{12}$, $\boldsymbol{u}_{21}$, $\boldsymbol{u}_{22}$ = 8×8 partitioned matrices.
U_i, U_o = imbalances of inner and outer rotors.
x_i, y_i , x_o, y_o = radial shaft displacements, m.
$\boldsymbol{Z}$ = 16×1 state vector with state variables: M_{yi}, Q_{xi}, M_{xi}, Q_{yi}, M_{yo}, Q_{xo}, M_{xo}, Q_{yo}, x_i, θ_{yi}, y_i, θ_{xi}, x_o, θ_{yo}, y_o, θ_{xo}.
α = cross-sectional shape factor for shear deformation of shaft.
Δ_1 = the frequency equation with singularity.
Δ_p = the non-singularity frequency equation.
θ_{xi}, θ_{xo} = angular displacement for inner and outer rotor in the *Y-Z* plane, rad.
θ_{yi}, θ_{yo} = angular displacement for inner and outer rotor in the *X-Z* plane, rad.
μ = poisson ratio.
ρ = density of shaft, kg/m^3
ω = precession angular velocity of the system, rad/s.
Ω = angular speed of shaft, rad/s.

Subscripts
a = lumped mass.
b = a massless elastic beam.
c = inter-bearing.
i = inner rotor.
k = station number.
o = outer rotor.
x = *X* direction in the *X-Z* plane.
y = *Y* direction in the *Y-Z* plane.

Superscripts
L = left-hand side of an element.
R = right-hand side of an element.